Available online at www.sciencedirect.com
ScienceDirect
Materials Research Bulletin 43 (2008) 2617–2625
Materials Research Bulletin
www.elsevier.com/locate/matresbu

The enhanced photoactivity of nanosized Bi_2WO_6 catalyst for the degradation of 4-chlorophenol

Hongbo Fu [a,b,*], Wenqing Yao [a], Liwu Zhang [a], Yongfa Zhu [a,**]

[a] Department of Chemistry, Tsinghua University, Beijing 100084, PR China
[b] Department of Environment Science and Engineering, Fudan University, Shanghai 200433, PR China

Received 1 June 2006; received in revised form 30 September 2007; accepted 29 October 2007
Available online 20 December 2007

Abstract

Nanosized Bi_2WO_6 catalyst exhibited the enhanced photoactivity for the degradation of 4-chlorophenol (4-CP) under visible irradiation compared to the sample prepared by high-temperature solid reaction. The photoactivity of the catalyst was sensitive to pH variation of the suspension. Nanosized Bi_2WO_6 catalyst showed the highest activity at pH 7.2. The photodegradation of 4-CP by nanosized Bi_2WO_6 catalyst followed a pseudo-first-order reaction. After three recycling runs for the photodegradation of 4-CP, the activity of the catalyst did not show any significant loss, suggesting that the catalyst was stable under visible irradiation.

Keywords: A. Nanostructures; A. Semiconductors; D. Surface properties

1. Introduction

Development of visible-light-driven photocatalyst for the decomposition of the environmental pollutants has been urged from the viewpoint of utilizing solar energy [1]. Although TiO_2 doped by nitrogen could degrade 4-CP under visible irradiation [2], the doping of N atoms also serves as sites for electron–hole recombination, resulting in a low quantum yield [3].

In oxide semiconductors, the conduction band levels of small band-gap semiconductors are usually low because the deep valence bands are formed by O 2p. This is a major problem for developing visible-light-driven photocatalysis. To find a breakthrough, it is indispensable to control the valence band with orbitals of some elements instead of O 2p. Bismuth is a potential candidate for such a valence-band-control element [4]. Recently, a great deal of efforts have been devoted to developing the photocatalysts containing bismuth with high activities for environmental applications and/or water splitting, such as $BiVO_4$ [5], $CaBi_2O_4$ [6], $Bi_2Ti_2O_7$ [7] and $Bi_4Ti_3O_{12}$ [8].

Bi_2WO_6 has been found to possess interesting physical properties such as ferro-electric piezoelectricity, pyroelectricity, catalytic behavior and non-linear dielectric susceptibility [9]. Recently, Kudo and Hijii [10] have reported that Bi_2WO_6 catalyst prepared by the solid-state reaction from the mixtures of WO_3 and Bi_2O_3 showed the

* Corresponding author at: Department of Environmental Science and Engineering, Fudan University, Shanghai 200433, PR China. Tel.: +86 6564 2526.
** Corresponding author at: Department of Chemistry, Tsinghua University, Beijing 100084, PR China. Tel.: +86 6278 7601.
E-mail addresses: fuhb@fudan.edu.cn (H. Fu), zhuyf@tsinghua.edu.cn (Y. Zhu).

0025-5408/$ – see front matter
doi:10.1016/j.materresbull.2007.10.044

photocatalytic activity for O_2 evolution from an aqueous silver nitrate solution under visible-light irradiation. More recently, Zou and coworkers [11] reported that Bi_2WO_6 catalyst prepared by the same method showed not only the activity for photocatalytic O_2 evolution but also the activity of mineralizing both $CHCl_3$ and CH_3CHO contaminants under visible-light irradiation. Therefore, the photocatalyst with a strong oxidizing potential could be postulated. Bi_2WO_6 photocatalysts were often prepared by the solid-state reaction [10,11] and the size of the crystal was situated in the microsized scope. It has been reported that nanostructured photocatalysts usually presented enhanced photocatalytic activities due to their special morphologies, high surface areas and high efficiency of electron–hole separation [12]. Up to date, there is only a little information about the photochemical properties of nanosized Bi_2WO_6, thus, it is an urgent need to study this photocatalyst.

In a previous work [4,13], we have successfully synthesized Bi_2WO_6 nanoplates by a simple hydrothermal process. The as-prepared sample shows high activity for the rhodamine B photodegradation. We reported herein that the nanosized Bi_2WO_6 was more active for the 4-CP photodegradation compared to N-doped TiO_2 and, in particular, exhibited an unusually high activity compared to the sample prepared by the solid-state reaction. Furthermore, the material was stable under irradiation. To the best of our knowledge, the photodegradation of 4-CP by nanosized Bi_2WO_6 catalyst was first investigated. Our work indicated that nanosized Bi_2WO_6 could photodegrade colorless compound under visible-light irradiation.

2. Experimental

2.1. Sample preparation and characterization

Nanosized Bi_2WO_6 was prepared by the hydrothermal synthesis method [4,13]. For comparison, the sample prepared by a high-temperature solid-state reaction and $TiO_{2-x}N_x$ sample ($x = 0.0488$) were prepared according to the previous literatures [2,11]. The x value (nitrogen concentration) in $TiO_{2-x}N_x$ was measured by X-ray photoelectron spectroscopy (XPS). XPS analysis were performed on a PHI 5300 ESCA instrument using an Al Kα X-ray source.

X-ray diffraction (XRD) with Cu Kα radiation was measured using a Bruker D8 Advance X-ray diffractometer. UV–vis diffused reflectance (DR) spectra of the samples were measured with a Hitachi U-3010 spectrometer. The spectra were recorded in the range 200–700 nm.

2.2. Photoreactor and light source

The light source was a 500 W xenon lamp (Institute of Electric Light Source, Beijing) positioned inside a cylindrical reaction vessel. The system was cooled by wind, and maintained the room temperature. An appropriate cutoff filter was placed upside the vessel to ensure complete removal of the radiation below 400 nm. The average light intensity was 40 mW cm^{-2}.

2.3. Procedure and analyses

Aqueous suspensions of 4-CP (10 mg L^{-1}) and Bi_2WO_6 powder (50 mg L^{-1}) were placed in a vessel. Prior to irradiation, the suspensions were magnetically stirred in the dark for ca. 30 min to ensure the establishment of the equilibrium. The suspensions were kept under constant air-equilibrated conditions before and during the irradiation. At given time intervals, 3 mL of aliquots were sampled, and centrifugated to remove the particles. The filtrates were analyzed by recording the variations of the absorption band (224 nm) in UV–vis spectra of the suspension using a Hitachi U-3010 spectrometer (Japan). Total organic carbon (TOC) was measured with a Tekmar Dohrmann Apollo 9000 TOC analyzer. Cl^- ion was analyzed with a Shimadzu LC-10AS ion chromatograph.

3. Results

3.1. Characterizations of the catalyst

The sheet-shaped crystal could be observed for the sample prepared by the hydrothermal process [4]. The sizes of crystals were not uniform and distributed in the scope of 50–200 nm. The large surface area was therefore expected.

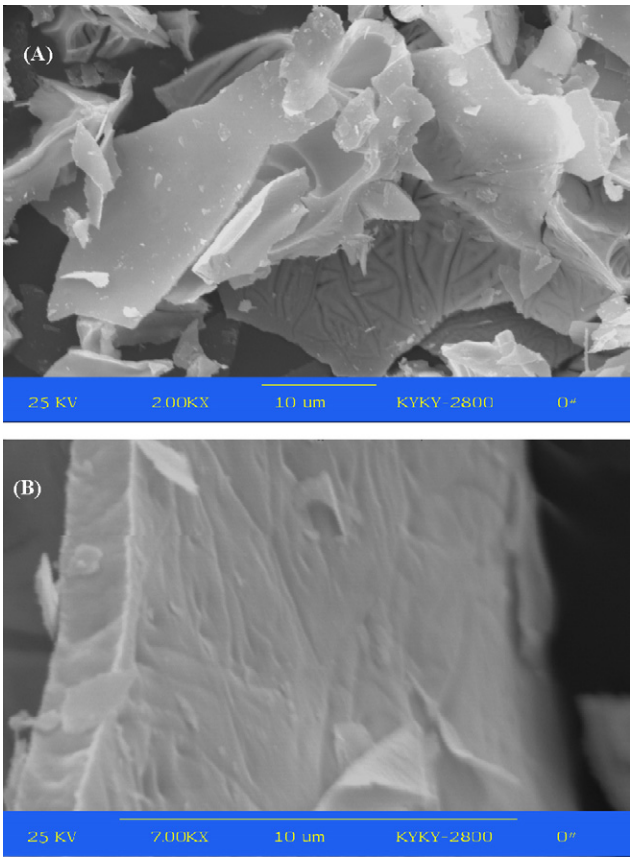

Fig. 1. SEM of the sample prepared by the solid-state reaction (A) and the amplified image of the sample prepared by the solid-state reaction (B).

SEM images of the sample prepared by the solid-state reaction are shown in Fig. 1A. The sample presented the tiled or curly plate-shaped morphology, the edges of which were often larger than 10 μm. The amplificatory image (Fig. 1B) shows the thickness of the plates exceeded to 0.5 μm. The surface area of the sample prepared by the hydrothermal process was 43.2 $m^2\ g^{-1}$, of which was by far larger than 0.69 $m^2\ g^{-1}$ of the sample by the solid-state reaction [11,13].

XRD pattern of the sample prepared by the hydrothermal process is shown in Fig. 2A. Bi_2WO_6, belong to the orthorhombic system, space group $Pca2_1$, and the crystal in a layered structure include the corner-shared WO_6. Bi atom layers are sandwiched between WO_6 octahedral layers [11]. After refinement, the cell constants of the sample were calculated to be $a = 5.456$ Å, $b = 5.436$ Å, $c = 16.426$ Å, which were consistent with the literature data and the standard card (JCPDS 73-1126) [11]. On the basis of the standard data, the intensity of the (1 1 3) peak is about five times than (2 0 0) or (0 2 0) peak which could be expressed as: $I_{113}/I_{200} = 5$. However, as for the sample prepared by the hydrothermal method, the value of I_{113}/I_{200} is almost less than 2, suggesting that the crystal has special anisotropic growth in (2 0 0) or (0 2 0) direction. These results could be attributed to their unique sheet-shaped morphologies [13].

Fig. 3 shows DR spectra of the samples prepared by the hydrothermal process and solid-state reaction, as well as N-doped TiO_2. Compared to the sample prepared by the solid-state reaction, the absorption of the sample prepared by the hydrothermal process appeared a blue shift. The band gap of the sample prepared by the hydrothermal process was estimated to be 2.75 eV from the onset of the absorption edge, which was wider than 2.69 eV of the sample prepared by the solid-state reaction [11]. This can be attributed to the nanosized effect. The steep shape of the spectra indicated that visible-light absorption was not due to the transition from the impurity level but was due to the band-gap transition. Nevertheless, the considerable absorption in the visible-light region was expected to be responsible for the photodegradation of the pollutants. The color of the sample prepared by the hydrothermal process was pale-yellow, as could be expected from the absorption spectrum. The absorption of N-doped TiO_2 in the visible-light region extended up to about 500 nm, which was in agreement with the previous report [2].

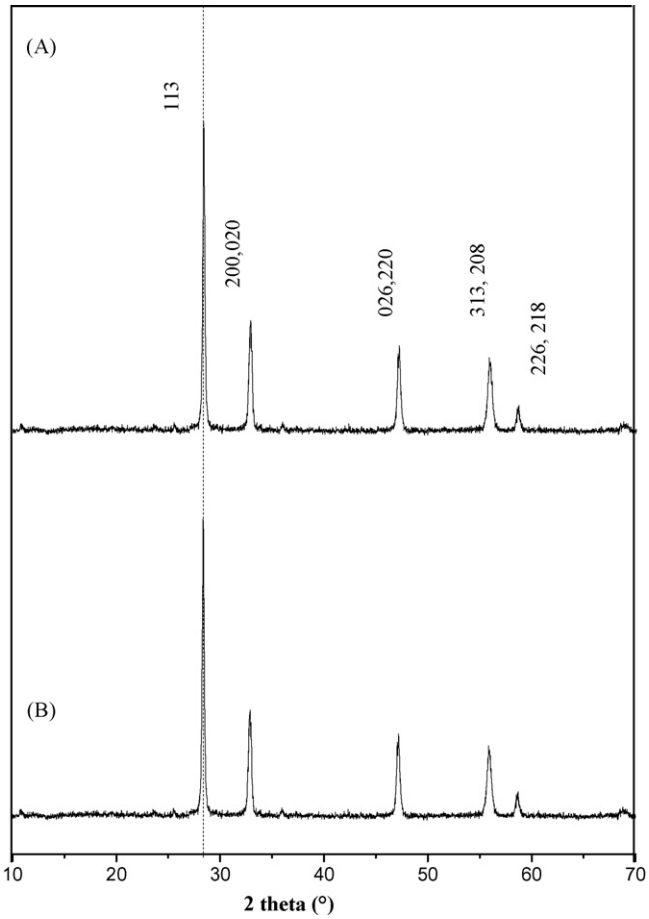

Fig. 2. XRD patterns of the sample prepared by the hydrothermal process before (A) and after (B) light irradiation ($\lambda > 400$ nm).

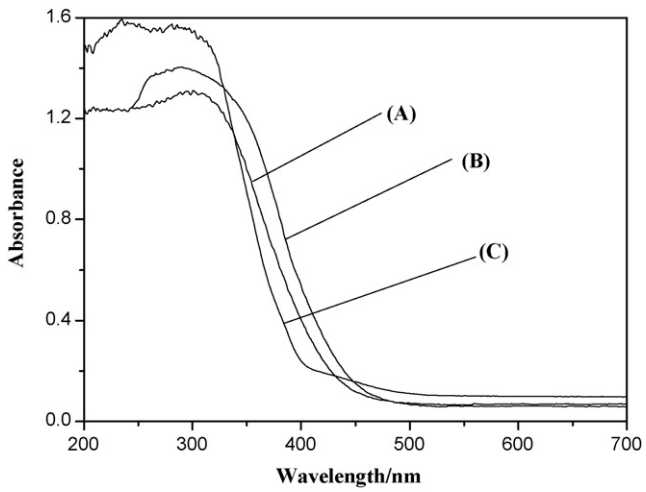

Fig. 3. DR spectra of the sample prepared by the hydrothermal process (A), the sample prepared by solid-state reaction (B) and N-doped TiO_2 (C).

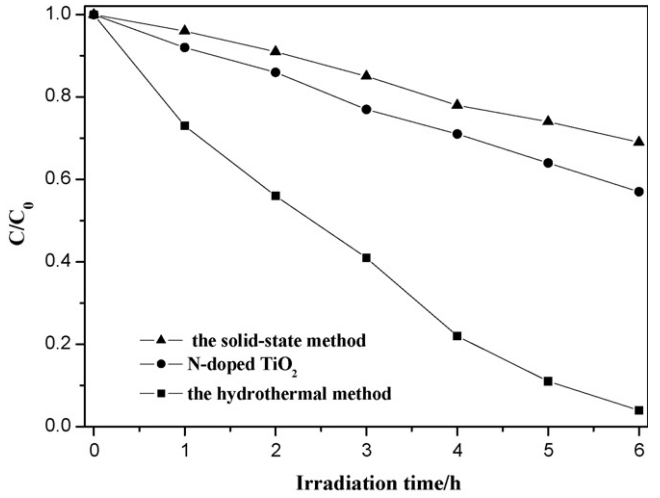

Fig. 4. The photodegradation of 4-CP in the presence of the different catalysts; catalyst loading, 0.5 g L^{-1}; the initial concentration of 4-CP, 10 mg L^{-1}; pH 7.2.

3.2. Photoactivity of the catalyst for the 4-CP degradation

The photocatalytic activity of the sample prepared by the hydrothermal process towards the degradation of 4-CP was then investigated. For comparison, the photodegradation of 4-CP by N-doped TiO_2 and the sample prepared by the solid-state reaction were also carried out. The results are shown in Fig. 4. The degradation of 4-CP was not significant at the absence of the catalyst under irradiation or in the presence of the catalyst in the dark (not shown). Nanosized Bi_2WO_6 showed the highest photoactivity for the 4-CP degradation under visible-light irradiation. Almost complete degradation of 4-CP was achieved in the presence of nanosized Bi_2WO_6 after 6 h. A 43% reduction of 4-CP in the concentration was observed in the presence of N-doped TiO_2. Only 31% reduction of 4-CP in the concentration were observed at the same time in the case of the sample prepared by the solid-state reaction.

The photodegradation of 4-CP over nanosized Bi_2WO_6 with the different initial pH are shown in Fig. 5. A variation in pH greatly influenced the photodegradation rate of 4-CP in Bi_2WO_6 suspension. Nanosized Bi_2WO_6 presented high photoactivity in the central pH solution. The fastest degradation was achieved at pH 7.2. A drastic decrease in the rate was found at pH 5.1 or pH 9.6, suggesting that the as-prepared sample was not stable in acidic or alkaline solution [4].

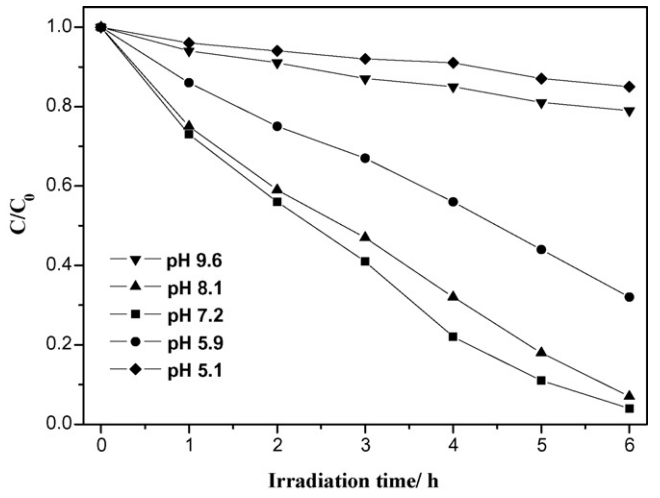

Fig. 5. The photodegradation of 4-CP in the presence of nanosized Bi_2WO_6 at different pH; catalyst loading, 0.5 g L^{-1}; the initial concentration of 4-CP, 10 mg L^{-1}.

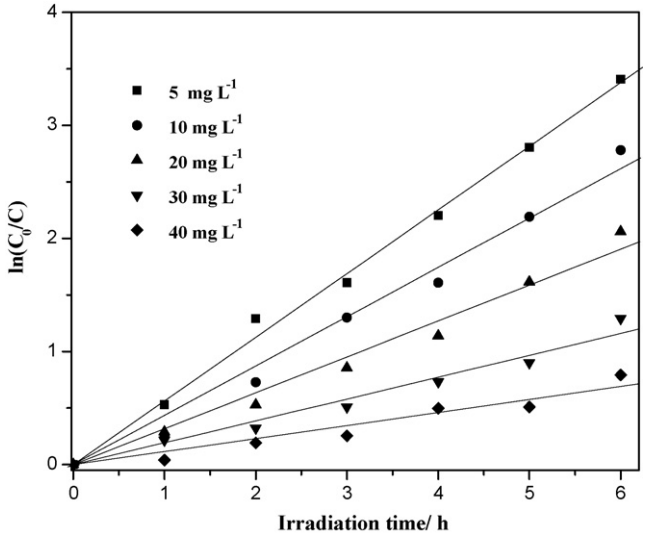

Fig. 6. First-order plots for the photodegradation of 4-CP by nanosized Bi_2WO_6 at various initial concentration; the suspensions containing 0.5 g L^{-1} Bi_2WO_6, pH 7.2, $\lambda > 400$ nm.

The influence of the initial concentration (C_0) on the photodegradation rate of 4-CP over nanosized $Bi_2WO_6$was also observed, and the results are shown in Fig. 6, in which the experimental data were fitted by applying a pseudo-first-order model $\ln(C/C_0) = -k_{obs}t$ to determine an observed rate constant (k_{obs}) of 4-CP reduction in the experiments. Via changing C_0 in the range 5–40 mg L^{-1}, the plots of irradiation time (t) *vs.* the ln C_0/C exhibited a nearly straight line, and the determined reaction rate constant (k) was 0.058, 0.052, 0.044, 0.034 and 0.020 h^{-1}, respectively, for the initial concentration of 4-CP of 5, 10, 20, 30, and 40 mg L^{-1}. It can be seen that the value of the rate constant (k_{obs}) varied significantly with the initial concentration of 4-CP, from 0.058 h^{-1} at 5 mg L^{-1} to 0.020 h^{-1} at 40 mg L^{-1}. The decrease of k_{obs} by increasing the 4-CP concentration can be explained by assuming competition between intermediates and substrate for the semiconductor active sites [14]. The above linear relationship could be explained in a Langmuir-Hinshelwood model [15], which presumes adsorption of substrate prior to its reaction on the surface:

$$r = \frac{-\mathrm{d}C}{\mathrm{d}t} = \frac{kKC}{(1+KC)} \tag{1}$$

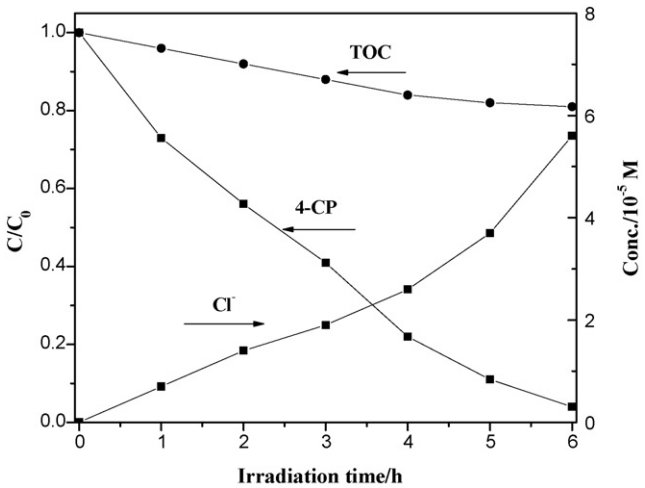

Fig. 7. Changes in 4-CP concentration and TOC and the formation of Cl^- during the course of the photodegradation of 4-CP (10 mg L^{-1}) in the presence of nanosized Bi_2WO_6 at pH 7.2.

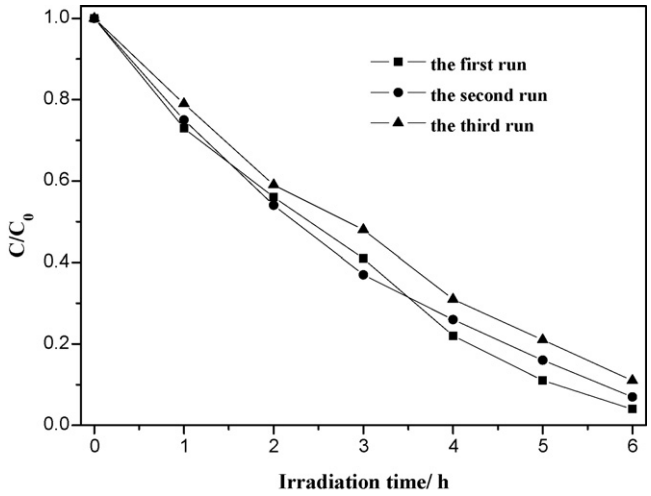

Fig. 8. Cycling runs for the photodegradation of 4-CP in the presence of nanosized Bi_2WO_6 under visible irradiation; catalyst loading, 0.5 g L^{-1}; the initial concentration of 4-CP, 10 mg L^{-1}; pH 7.2.

where r is the oxidation rate of the reactant (mg L^{-1} h^{-1}), C the concentration of reactant (mg L^{-1}), t the illumination time, k the reaction rate constant (mg L^{-1} h^{-1}), and K is the adsorption coefficient of the reactant (L mg^{-1}).

The decrease of TOC and the formation of Cl^- in the photodegradation of 4-CP by nanosized Bi_2WO_6 were also performed. The results are shown in Fig. 7. The rate of TOC reduction was remarkably slower than that of 4-CP. About 80% of TOC still remained in the suspension after 6 h irradiation while 4-CP was almost completely degraded. After 6 h irradiation, the concentration of Cl^- rose to reach 71.9% (5.6×10^{-5} M) of the theoretical quantity (7.8×10^{-5} M). It can be concluded from this result that the most degradation of 4-CP could be only a dechlorine process.

Bi_2WO_6 as a kind of heterogeneous photocatalyst could be easily recycled by a simple filtration because its large density (9.505 g cm^{-3}). After three recycles for the photodegradation of 4-CP, the activity of the catalyst did not exhibit any significant loss, as shown in Fig. 8, confirming the as-prepared sample was stable during the photocatalytic oxidation of the pollutant molecules. XRD analysis of the sample also showed that the crystal structure of the photocatalyst was not changed after the photocatalytic reaction (Fig. 2B). The stability of the photocatalyst may be related to the condition of hydrothermal synthesis. The hydrothermal method allows the crystallization of catalyst under mild conditions over a long period of time. The catalyst crystallizing in the water medium of hydrothermal condition indicates that it could show a stable photoactivity for the photodegradation of organic pollutants [16].

4. Discussion

The energy level and the band gap of the oxide semiconductor play a crucial role in determining photocatalytic activity. The band structure of the tungstate semiconductors is generally defined by the W 5d level and the O 2p level. In such case, the characteristic absorption under visible-light region is impossible due to the fact that the flat-band potentials of the O 2p level and the W 5d level are 2.94 eV (SHE) and −0.37 eV (SHE), respectively [4,6,16]. However, in the case of Bi_2WO_6, the transition of the 6s electrons of Bi^{3+} to the empty 5d orbitals of W^{6+} become possible. Such a transition has been also observed in $BiVO_4$ [5]. This transition due to the 6s electrons usually occurs at a lower energy than the charge-transfer transition in WO_6^{6-}. As a result, the valence band of Bi_2WO_6 may be formed by not noly O 2p but also Bi 6s, namely the hybrid orbitals of Bi 6s and O 2p [4]. Therefore, Bi_2WO_6 possesses at least two absorption bands in UV and visible region. The absorption band in the visible-light region is contributed to the visible photocatalytic activity.

In the most of the proposed mechanisms for the photodegradations of organic pollutants by the semiconductors, the highly oxidizing (surface-bound) hydroxyl radical, which originates from the oxidation of chemisorbed OH^- or H_2O by the photogenerated valence band holes, is regarded as the main oxidative species responsible for the degradation [12]. No doubt some reactions can also be initiated by a direct hole oxidation, especially when the adsorption of the

substrates is rather extensive and the concentrations of the substrates are relatively high [17,18]. Photooxidation of the pollutant over nanosized Bi_2WO_6 photocatalyst occurs as a result of contributions from the photoexcited holes in the valence band consisting of the O 2p and Bi 6s hybrid orbitals. When the Bi^{3+} ion forms a valence band, the holes formed by photoexcitation are regarded as Bi^{5+} (or Bi^{4+}). Although a redox potential in an aqueous solution is different from that in solid, a stand redox potential of Bi_2O_4/BiO^+ (Bi^V/Bi^{III}) (E° = + 1.59 eV at pH 0) could make sense for a rough estimation of the oxidation potential of the hole (Bi^{5+}) photogenerated in Bi_2WO_6 photocatalyst [19]. The standard redox potential of Bi^V/Bi^{III} is more negative than that of $OH^\bullet/OH^-$(+1.99) [20], suggesting that the hole photogenerated on the surface of Bi_2WO_6 could not react with OH^-/H_2O to form $^\bullet OH$. Therefore, the decomposition of 4-CP by Bi_2WO_6 catalyst could be due to the reaction with the photogenerated hole directly. The potential of the holes is sufficient to photocatalytic activity for O_2 evolution from water [10], to oxidize $CHCl_3$ and CH_3CHO [11], and to photocatalytic dechlorine of 4-CP from the present study.

Nanosized Bi_2WO_6 has a priority to exert its photochemical activity due to its large surface area. Generally, e^-/h^+ recombination in the materials is divided into two categories: the volume recombination and the surface recombination. The volume recombination is a dominant process in well-crystallized bulk materials and is reduced by increasing the surface area of large particles. A larger surface area increases the available surface active sites and could lead to a higher photonic efficiency. The BET specific surface area of the sample prepared by the hydrothermal process is improved by about 60 times as compared to the sample prepared by the solid-state reaction [11,13]. The surface e^-/h^+ recombination is mainly due to the abundant surface trapping sites and an insufficient driving force for e^-/h^+ pair separation [20]. Thus, the highly photocatalytic efficiency of nanosized Bi_2WO_6 catalyst is expected by accelerating the interfacial charge carrier transfer processes, increasing the amount of the adsorbed 4-CP. Apart from the enhanced surface area, nanosized Bi_2WO_6 catalyst is expected to have the stronger oxidizing potential due to the nanosized effect. This could be the important reason why it exhibited the enhanced photoactivity.

A unique sheet structure is beneficial to the transfer of electrons from the bulk to the surface of the photocatalyst. It was reported that a series of the sheet-shaped materials showed high activity for water splitting under irradiation. The sheet-shaped structure was found to promote the generation and the separation of the charge carriers [21]. More importantly, the sample prepared under the mild hydrothermal condition hold higher crystallinity as compared to the sample prepared at high temperature. In general, the higher the crystallinity was, the higher the photocatalytic activity was, because the recombination between photogenerated electrons and holes was suppressed in the highly crystalline photocatalysts. The low crystallinity of the sample prepared by the solid-state reaction leaded to the lower photocatalytic activity due to a quantity of vacancy sites.

5. Conclusions

Nanosized Bi_2WO_6 exhibited the stronger capability to photocatalytic degradation of 4-CP as compared to the sample prepared by the solid-state reaction and N-doped TiO_2. The photoactivity of nanosized Bi_2WO_6 catalyst was sensitive to pH variation of the solution, and the catalyst showed high activity in the central pH solution. The as-prepared sample was stable under visible irradiation.

Acknowledgments

This work was partly supported by Chinese National Science Foundation (20433010, 20571047) and Trans-Century Training Program Foundation for the Talents by the Ministry of Education, PR China, and China Postdoctoral Science Foundation (2005037050) for financial support.

References

[1] Z. Zou, J. Ye, K. Sayama, H. Arakawa, Nature 414 (2001) 625.
[2] H. Fu, L. Zhang, S. Zhang, Y. Zhu, J. Phys. Chem. B 110 (2006) 3061.
[3] M. Mrowetz, W. Balcerski, A.J. Colussi, M.R. Hoffmann, J. Phys. Chem. B 108 (2004) 45.
[4] H. Fu, C. Pan, W. Yao, Y. Zhu, J. Phys. Chem. B 109 (2005) 22432.
[5] S. Tokunaga, H. Kato, A. Kudo, Chem. Mater. 13 (2001) 4624.
[6] H. Fu, C. Pan, L. Zhang, Y. Zhu, Mater. Res. Bull. 42 (2007) 696.
[7] W. Yao, H. Wang, X. Xu, J. Zhou, X. Yang, Y. Zhang, S. Shang, Appl. Catal. A-Gen. 259 (2004) 29.

[8] W. Yao, X. Xu, H. Wang, J. Zhou, X. Yang, S. Shang, B. Huang, Appl. Catal. B-Environ. 52 (2004) 109.
[9] Y. Shi, S. Feng, C. Cao, Mater. Lett. 44 (2000) 215.
[10] A. Kudo, S. Hijii, Chem. Lett. (1999) 1103.
[11] J. Tang, Z. Zou, J. Ye, Catal. Lett. 92 (2004) 53.
[12] M.R. Hoffmann, S.T. Martin, W. Choi, Chem. Rev. 95 (1995) 69.
[13] H. Fu, L. Zhang, W. Yao, Y. Zhu, Appl. Catal. B Environ. 66 (2006) 100.
[14] C. Hong, Y. Wang, B. Bush, Chemosphere 36 (1998) 1653.
[15] I.K. Konstantinou, T.A. Albanis, Appl. Catal. B-Environ. 49 (2004) 1.
[16] H. Fu, J. Lin, L. Zhang, Y. Zhu., Appl. Catal. A-Gen. 306 (2006) 58.
[17] M.A. Fox, M.T. Dulay, Chem. Rev. 93 (1993) 341.
[18] H. Fu, X. Quan, Z. Liu, S. Chen, Langmuir 20 (2004) 4867.
[19] N. Bao, X. Feng, Z. Yang, L. Shen, X. Lu, Environ. Sci. Technol. 38 (2004) 2729.
[20] E. Yasuo, S. Takayoshi, H. Masaru, W. Mamoru, Chem. Mater. 14 (2002) 4309.
[21] M. Mrowetz, W. Balcerski, A.J. Colussi, M.R. Hoffmann, J. Phys. Chem. B 108 (2004) 17270.